Cyclodextrins increase membrane tension and are universal activators of mechanosensitive channels

Charles D. Cox[a,b,1], Yixiao Zhang[c,2], Zijing Zhou[a], Thomas Walz[c], and Boris Martinac[a,b]

[a]Molecular Cardiology and Biophysics Division, Victor Chang Cardiac Research Institute, Sydney, NSW 2010, Australia; [b]St Vincent's Clinical School, Faculty of Medicine, University of New South Wales, Sydney, NSW 2010, Australia; and [c]Laboratory of Molecular Electron Microscopy, The Rockefeller University, New York, NY 10065

Edited by Ardem Patapoutian, The Scripps Research Institute, La Jolla, CA, and approved July 29, 2021 (received for review March 14, 2021)

The bacterial mechanosensitive channel of small conductance (MscS) has been extensively studied to understand how mechanical forces are converted into the conformational changes that underlie mechanosensitive (MS) channel gating. We showed that lipid removal by β-cyclodextrin can mimic membrane tension. Here, we show that all cyclodextrins (CDs) can activate reconstituted *Escherichia coli* MscS, that MscS activation by CDs depends on CD-mediated lipid removal, and that the CD amount required to gate MscS scales with the channel's sensitivity to membrane tension. Importantly, cholesterol-loaded CDs do not activate MscS. CD-mediated lipid removal ultimately causes MscS desensitization, which we show is affected by the lipid environment. While many MS channels respond to membrane forces, generalized by the "force-from-lipids" principle, their different molecular architectures suggest that they use unique ways to convert mechanical forces into conformational changes. To test whether CDs can also be used to activate other MS channels, we chose to investigate the mechanosensitive channel of large conductance (MscL) and demonstrate that CDs can also activate this structurally unrelated channel. Since CDs can open the least tension-sensitive MS channel, MscL, they should be able to open any MS channel that responds to membrane tension. Thus, CDs emerge as a universal tool for the structural and functional characterization of unrelated MS channels.

methyl-β-cyclodextrin | phospholipids | cryo–electron microscopy | patch clamp

Bacterial mechanosensitive (MS) channels have been extensively used as models of ion channel–mediated mechanotransduction (1, 2). They have continually provided novel insights into the biophysical principles that govern ion-channel mechanosensitivity (3–6). While the structurally unrelated MS channels MscL (mechanosensitive channel of large conductance) (4) and MscS (mechanosensitive channel of small conductance) (7) both respond to changes in membrane tension (8–10), at the molecular level, they seem to employ different strategies to convert membrane forces into the conformational changes that underlie channel gating.

Escherichia coli MscS is the archetypal member of a large structurally diverse family of ion channels that are expressed in bacteria (11, 12), archaea (13), some fungi (14), plants (15, 16), and eukaryotic parasites (17). This channel gates as a result of membrane tension (10) in accordance with the "force-from-lipids" gating mechanism (6). In response to increases in membrane tension, MscS exhibits complex adaptive gating kinetics (18–20). These kinetic responses may represent two separable processes, adaptation and inactivation (21, 22). In particular, point mutations within transmembrane domain 3 can instigate phenotypes in which adaptation and inactivation are affected differently (18, 23, 24). These complex kinetics are important for the role of this channel as an osmotic safety valve (25). However, since it is currently unknown whether these electrophysiologically separable processes correlate to structurally distinct states, we will refer to them collectively as "desensitization." In addition, while some data suggest that MscS desensitization is sensitive to the lipid environment (26), this notion still awaits definitive proof.

MscL was the first MS channel to be cloned and functionally characterized in a lipid-only environment (8). Members of the MscL family, unlike those of the MscS family, are almost exclusively expressed in archaea and bacteria. After X-ray crystallography revealed the structure of MscL (27), subsequent studies implicated membrane thinning in response to membrane tension as a major driver of MscL gating (3, 28).

To fully understand the structural basis of the gating transitions in MscL and MscS, one must first find a way to apply a gating stimulus to the channels in a lipidic environment that is compatible with structural studies. This is, of course, less challenging when considering ligand-gated channels (29–31), for which the stimulus is a defined molecule that can readily be applied to visualize the resulting changes in protein conformation. For MS channels, until recently, only spectroscopic approaches, such as electron paramagnetic resonance spectroscopy (32, 33) and Förster resonance energy transfer spectroscopy (34, 35), were available to provide structural insights into their gating in response to changes in forces in their lipid environment. Other approaches had been confined to the use of activators (36) or mutations (37, 38). We recently demonstrated that lipid removal by β-cyclodextrin can mimic membrane tension in membrane-scaffold protein-based lipid nanodiscs, providing novel insights into the structural rearrangements that underlie MscS channel

Significance

Mechanosensitive (MS) channels play a key role in the physiology of organisms from bacteria to man. Many prokaryotic and eukaryotic MS channels respond to membrane tension. Here, we show that cyclodextrin (CD)–mediated lipid removal induces membrane tension that activates not only the mechanosensitive channel of small conductance but the structurally unrelated mechanosensitive channel of large conductance, which gates at almost lytic membrane tensions. This finding suggests that for both functional and structural studies, provided that sufficient CD is added and enough lipids are removed, any tension-sensitive ion channel can be activated. Moreover, CDs may also prove useful for the in vitro study of other membrane proteins that are sensitive to mechanical forces.

Author contributions: C.D.C., Y.Z., T.W., and B.M. designed research; C.D.C., Y.Z., and Z.Z. performed research; C.D.C., Y.Z., T.W., and B.M. contributed new reagents/analytic tools; C.D.C., Z.Z., and T.W. analyzed data; and C.D.C., Y.Z., T.W., and B.M. wrote the paper.

The authors declare no competing interest.

This article is a PNAS Direct Submission.

[1]To whom correspondence may be addressed. Email: c.cox@victorchang.edu.au.

[2]Present address: Interdisciplinary Research Center of Biology and Chemistry, Shanghai Institute on Organic Chemistry, Chinese Academy of Sciences, Shanghai 200032, China.

This article contains supporting information online at https://www.pnas.org/lookup/suppl/doi:10.1073/pnas.2104820118/-/DCSupplemental.

Published September 2, 2021.

gating in response to membrane tension (39). The idea was that, as long as the surface area would not change and the lipids would not be replaced, β-cyclodextrin–mediated lipid removal from a membrane would result in the remaining lipids having to cover a larger surface area. This increase in "area-per-lipid" would result in a corresponding increase in membrane tension (40, 41) that would be experienced by integral membrane proteins incorporated in that membrane.

Cyclodextrins (CDs) are a family of cyclic glucose oligomers with a cone-like three-dimensional architecture characterized by a polar external surface and a hydrophobic cavity (42, 43). α-, β-, and γ-CD contain six to eight glucose units, respectively. As the number of units increases, so does the diameter of the hydrophobic cavity (5 to 8 Å) (43). These compounds are of broad utility, as the hydrophobic cavity can chelate a plethora of small lipophilic molecules (44, 45). CDs can also form complexes with fatty acids and phospholipids (46). CDs have thus been widely used to remove lipids from native cell membranes (47, 48) and from model membranes (49, 50). This removal of lipids has already been directly linked to increases in membrane tension even in intact cellular environments (51). CDs also exhibit differential lipid selectivity. For example, α-CD has the selectivity profile of phosphatidylserine > phosphatidylethanolamine >> phosphatidylcholine (52). The methylated version of β-CD (mβ-CD) shows selectivity toward cholesterol at low concentrations and has been widely used to selectively remove or add cholesterol to cell membranes (48, 53–55). In addition to the headgroup, CDs also preferentially chelate unsaturated lipids and those containing shorter acyl chains (56, 57).

Here, we show that all members of the CD family (α, β, and γ) can activate *E. coli* MscS in liposomal membranes. Even the methylated version of β-CD, which is widely used for its cholesterol selectivity, can activate *E. coli* MscS. Congruent with lipid removal increasing tension, the CD amount required for the activation of an MS channel depends on its tension sensitivity. Importantly, as a control, cholesterol-loaded CDs do not activate MscS. Our studies also clearly establish that MscS desensitization is modified by the lipid environment. Moreover, we show that CD-mediated lipid removal causes a concentration- and time-dependent increase in the tension in excised membrane patches and that the resulting tension can become sufficiently high to activate the structurally unrelated MS channel MscL that gates at membrane tensions immediately below the lytic limit of membranes. Two-dimensional (2D) class averages of nanodisc-embedded MscL obtained by cryo–electron microscopy (cryo-EM) indicate that β-CD treatment results in membrane thinning and channel expansion. The fact that CD activates MscL, which opens immediately below the lytic tension of the membrane, suggests that all other MS channels (which are all more sensitive to membrane tension) should also open in response to CDs. These data suggest that CDs will be of broad utility for the structural and functional characterization of structurally diverse MS channels, including Piezo channels (58, 59), two-pore domain K^+ channels (40, 60), and OSCA channels (61, 62), all of which are known to respond to membrane forces.

Results

All CDs Activate MscS Reconstituted into Azolectin Liposomes. We first tested whether all CDs could activate wild-type MscS. For this purpose, we purified N-terminally 6xHis-tagged MscS (6xHis-MscS) and reconstituted it into azolectin liposomes using the dehydration/rehydration (D/R) method. The electrophysiological properties of 6xHis-MscS have been reported to differ from those of C-terminally His-tagged or untagged MscS (63). Nevertheless, 6xHis-MscS reconstituted into azolectin liposomes produced stretch-evoked currents with a sensitivity similar to that of MscS after removal of the N-terminal 6xHis tag. However, since 6xHis-MscS displayed pronounced irreversible desensitization behavior (*SI Appendix*, Fig. S1 *A–C*), the N-terminal 6xHis tag was cleaved off for all further experiments.

The application of α-, β-, and γ-CD (10 mM) to excised liposome patches activated the incorporated MscS in the absence of any applied hydrostatic pressure (Fig. 1 *A–D*). Activation occurred rapidly with all three CDs, namely within 45 s of perfusion (combined $n = 19$). In most cases, activity was induced within 10 s, and the variabilities observed in the time to first activation, as seen in the representative traces shown in Fig. 1 *B–E*, are quantified in Table 1. Once the first channel opened, all the remaining channels in the patch opened within a short time frame, ~ seconds (Table 1). We observed little difference in the time course of activation elicited by the different CDs (Table 1), and with all CDs we observed instances of channel desensitization prior to membrane rupture, as exemplified in Fig. 1*C*.

Activation also occurred with the methylated derivative of β-CD (10 mM mβ-CD), which is often used to extract cholesterol from membranes (Fig. 1*E*). In contrast, application of the same concentration of mβ-CD (10 mM) that was saturated with cholesterol did not induce MscS gating (Fig. 1 *E–G*). In fact, perfusion of cholesterol-saturated mβ-CD reduced the sensitivity of MscS as evidenced by a rightward shift in the pressure-response curve that was recorded 3 min after the cholesterol-saturated mβ-CD was added (Fig. 1 *G* and *H*). This observation suggests that cholesterol was transferred from mβ-CD into the membrane patch, as cholesterol has previously been shown to reduce the mechanosensitivity of *E. coli* MscS (64). Together, these results strongly support the notion that CDs activate MscS by creating membrane tension as a result of removing lipids from the membrane, whereas inserting additional lipids, in particular cholesterol that further reduces membrane fluidity and increases membrane stiffness by intercalating in between the lipid acyl chains, creates membrane pressure that inhibits MscS.

Sustained membrane tension in response to the application of negative pressure has previously been reported to induce multiple long-lived substates in MscS (65). The addition of CDs also resulted in prolonged sojourns of MscS into substates (*SI Appendix*, Fig. S2 *A–C*), supporting the notion that CDs generate sustained elevated membrane tension. In addition, we proposed that the structure of MscS in the open state is dynamic (39), and the multiple substates observed here support this view.

CD Removes Lipids from Excised Liposome Patches. To further corroborate that MscS activation by CDs is due to lipid removal, we perfused membrane patches with CDs and concomitantly recorded MscS activation and imaged the patch membrane. The fluorescent lipid rhodamine-PE18:1 was added to both visualize the patch and monitor the lipid content. In empty liposomes with no channel protein incorporated, perfusion with 5 or 10 mM β-CD caused a graded reduction in fluorescence intensity within the patch (Fig. 2*A*). No quantal events signifying channel openings were observed up until the patch ruptured. In patches containing MscS, we observed that MscS activity occurred concomitantly with a reduction in the dome height of the liposome patch (Fig. 2 *B–D*). This flattening of the dome was evident when the dome height was measured over time (Fig. 2 *C* and *D*). The resting inward curvature seen at the beginning of the recordings is only possible in the presence of excess lipids. As the lipids were removed, the patch membrane flattened, and this coincided with channel activation (Fig. 2*B*). We quantified the degree of flattening in control experiments in which no β-CD was added in comparison to the level of flattening induced by 10 mM β-CD which, coincided with MscS activation (Fig. 2*D*).

The Amount of CD Required to Activate MscS Scales with Its Sensitivity to Membrane Tension. The tension sensitivity of MscS is affected not only by mutations but also by the lipid composition of the surrounding membrane (26, 64). We recently reported that

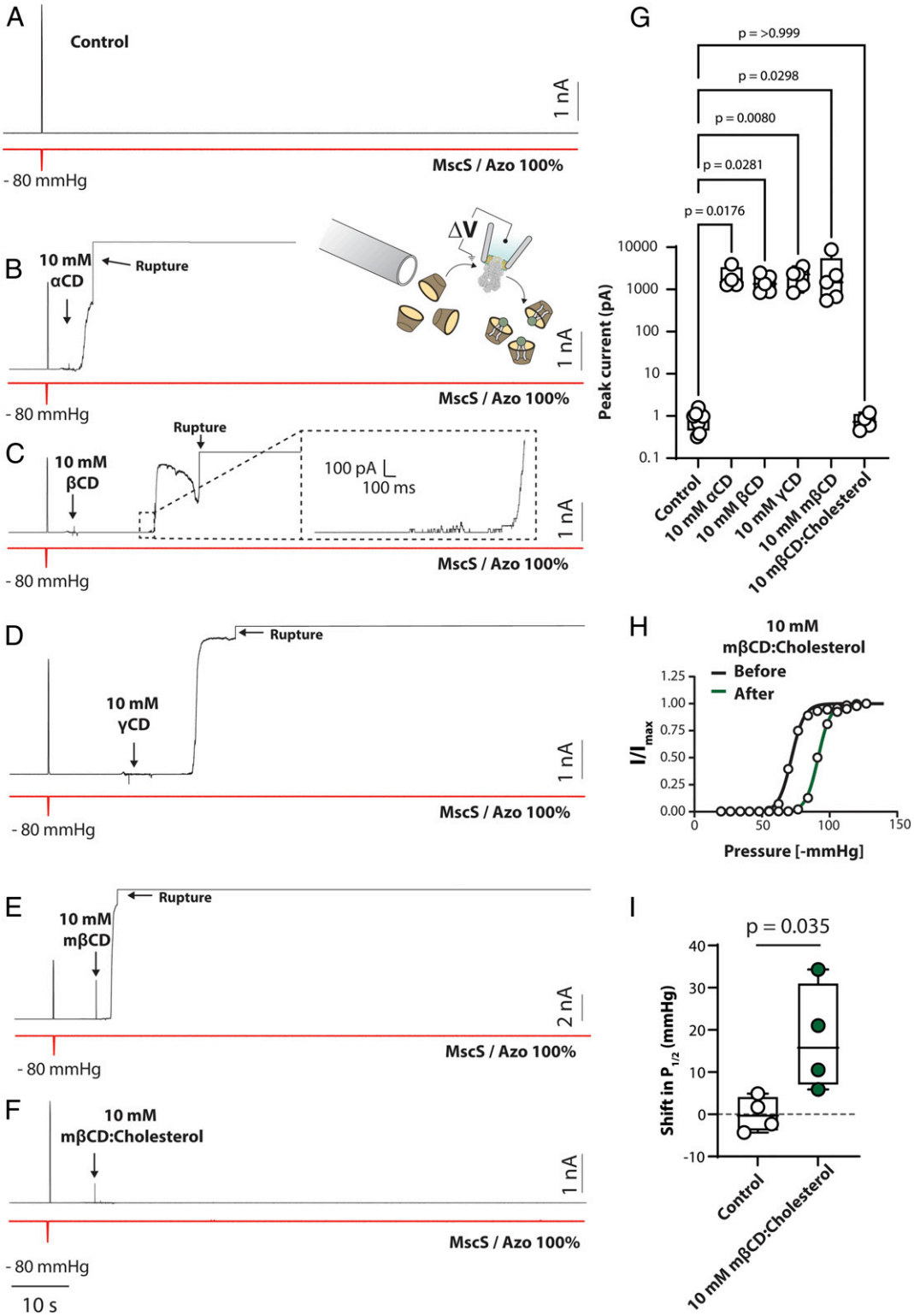

Fig. 1. CDs activate MscS reconstituted into azolectin bilayers. (*A*) Representative control patch-clamp recording of MscS reconstituted into azolectin (Azo) liposomes (1:200 protein:lipid ratio) at +20 mV pipette potential. The red trace shows the application of negative hydrostatic pressure with a 100-ms ramp up to −80 mmHg. (*B–F*) Representative patch-clamp recordings of MscS reconstituted into azolectin liposomes in response to perfusion of 10 mM α-CD (*B*), 10 mM β-CD (*C*), 10 mM γ-CD (*D*), 10 mM mβ-CD (*E*), and 10 mM mβ-CD loaded with cholesterol (mβ-CD:cholesterol) (*F*). These recordings show that all CDs and their derivatives can activate MscS in azolectin liposomes. Note that for all CDs, some traces showed evidence of MscS desensitization, as clearly seen in *C*. (*G*) Quantification of the peak current elicited from excised liposome patches in response to CD perfusion prior to patch rupture. *P* values shown were generated by comparison to the control group (not perfused) according to the Kruskal–Wallis test with Dunn's post hoc. (*H*) Representative Boltzmann fit of MscS pressure response before (black) and after (green) the perfusion of 10 mM mβ-CD:cholesterol. The rightward shift in the pressure-response curve indicates that the channel is less sensitive to applied force. (*I*) Quantification of the degree of rightward shift in the pressure-response curve of MscS patches not perfused with mβ-CD:cholesterol (control) compared with those perfused with 10 mM mβ-CD:cholesterol (*t* test used for comparison). Data are represented as minimum to maximum box and whisker plots showing all data points.

Table 1. Temporal information for the activation of MscS in azolectin patches treated with 10 mM of the respective cyclodextrins

Cyclodextrin type (10 mM)	Time to first opening (s)	Time from first opening to peak current (s)
αCD	5.62 ± 2.64 (n = 4)	1.01 ± 0.22 (n = 4)
βCD	3.39 ± 1.90 (n = 5)	1.17 ± 0.26 (n = 5)
γCD	5.36 ± 2.55 (n = 5)	1.36 ± 0.21 (n = 5)
mβCD	5.69 ± 3.38 (n = 5)	1.56 ± 0.20 (n = 5)

Data represent mean ± SEM.

doping azolectin liposomes with 30% (weight [wt]/wt) PC10 (1,2-didecanoyl-*sn*-glycero-3-phosphocholine), a lipid with two short 10-carbon acyl chains, causes spontaneous short-lived substate openings of MscS (39). While electrophysiological (26, 64) and structural data (39) suggest hydrophobic mismatch is not the main driver of MscS channel gating, we found that as little as 15% PC10 does increase the tension sensitivity of MscS (Fig. 3 *A*–*C*). In addition, we observed that PC10 substantially slowed channel closure, with MscS remaining open for seconds after hydrostatic pressure had returned to zero (Fig. 3 *A* and *D*).

The membrane tension will increase with the number of lipids that are removed by CDs, because each remaining lipid will have to occupy an increasingly larger surface area (40, 41). We therefore hypothesized that, in lipid environments in which MscS is more sensitive to membrane tension, fewer lipids would need to be removed by CDs to generate sufficient tension to open the channel (i.e., less β-CD should be necessary to open the channel). To test this hypothesis, we compared the effect of much lower amounts of β-CD (<10 mM) on MscS activity in liposomes containing 15% PC10. In such a membrane environment, MscS was indeed activated by β-CD concentrations as low as 750 μM (Fig. 3 *A* and *D*). In comparison, over the same electrophysiological recording period, 750 μM β-CD failed to elicit any gating events for MscS that was incorporated in azolectin liposomes that contained no PC10.

CD-Induced Activation Reveals that MscS Desensitization Is Affected by the Lipid Environment. As shown in Fig. 1*C*, β-CD induces MscS activation followed by desensitization. *E. coli* membranes are predominantly composed of phosphatidylethanolamine (PE) lipids. Thus, to more closely mimic the native lipid environment (66) of the channel and to examine the effect of membrane composition on MscS desensitization, we reconstituted MscS into pure azolectin liposomes and liposomes made of 70% azolectin with 30% PE18:1 (1,2-dioleoyl-*sn*-glycero-3-phosphoethanolamine). Incorporation of MscS into liposomes containing 70% azolectin and 30% PE18:1 right-shifted the pressure response of MscS ($P_{1/2}$ = 71.1; 95% confidence interval [CI]: 70 to 74.5) compared to channels reconstituted into pure azolectin liposomes ($P_{1/2}$ = 53.9; 95% CI: 51.5 to 56.1). Fig. 3 shows that lower amounts of β-CD were required to generate MscS activity when the channel was reconstituted into PC10-containing liposomes, in which case, lower tensions sufficed to open MscS. Consistent with this result, more β-CD was required (i.e., 15 mM) to elicit gating events in liposomes doped with 30% PE18:1 (Fig. 4*A*), in which case, higher tensions are needed to open MscS. Lower β-CD amounts failed to elicit MscS activity in liposomes with 30% PE18:1 (0/6 patches with 5 mM β-CD) over the same recording period (90 s). Moreover, after activation of MscS in liposomes doped with 30% PE18:1, we observed rapid full desensitization of the channel (Fig. 4*A*). Conversely, Gly113Ala mutant MscS, which displays abrogated desensitization (23, 24), was activated by lower concentrations of β-CD (e.g., 5 mM), even in liposomes containing 30% PE18:1. This mutant stayed open for long periods (>10 s), with little to no evidence of desensitization (Fig. 4 *B* and *C*). This result provides further support for the notion that CD treatment induces sustained membrane tension that maintains Gly113Ala mutant MscS in the open state for long periods. Importantly, as

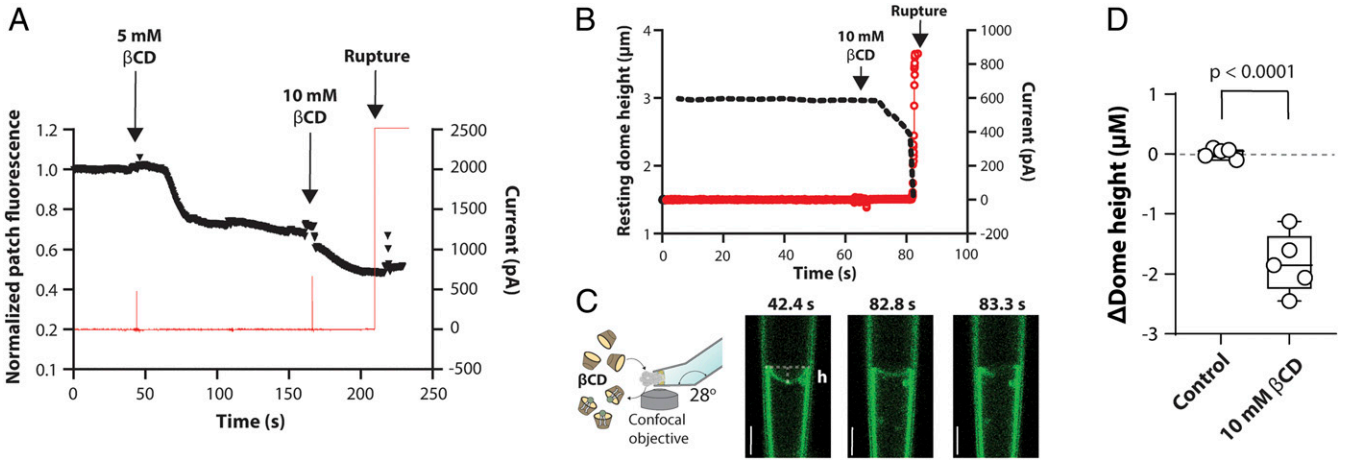

Fig. 2. β-CD removes lipids from excised membrane patches. (*A*) Normalized patch fluorescence of an azolectin liposome patch containing 0.1% rhodamine-PE (black) without any reconstituted channels. Red trace shows concomitant electrophysiology trace showing no channel activity and ultimate patch rupture. (*B*) Height of the patch dome measured concomitantly with electrophysiological recording of the activity of MscS reconstituted into azolectin liposomes supplemented with 0.1% rhodamine-PE. Black trace shows how the dome height changes with time, and red trace represents channel current. Time point when 10 mM β-CD was added is indicated. (*C*) Cartoon illustrating the experimental set up (*Left*) with representative confocal images of the patch dome during patch-clamp recordings at indicated time points (*Right*) from the time course shown in *B*. h denotes the height of the dome. (Scale bars, 5 μm.) (*D*) Minimum to maximum box and whisker plots showing the change in dome height after β-CD addition compared with no addition (P < 0.0001, unpaired t test).

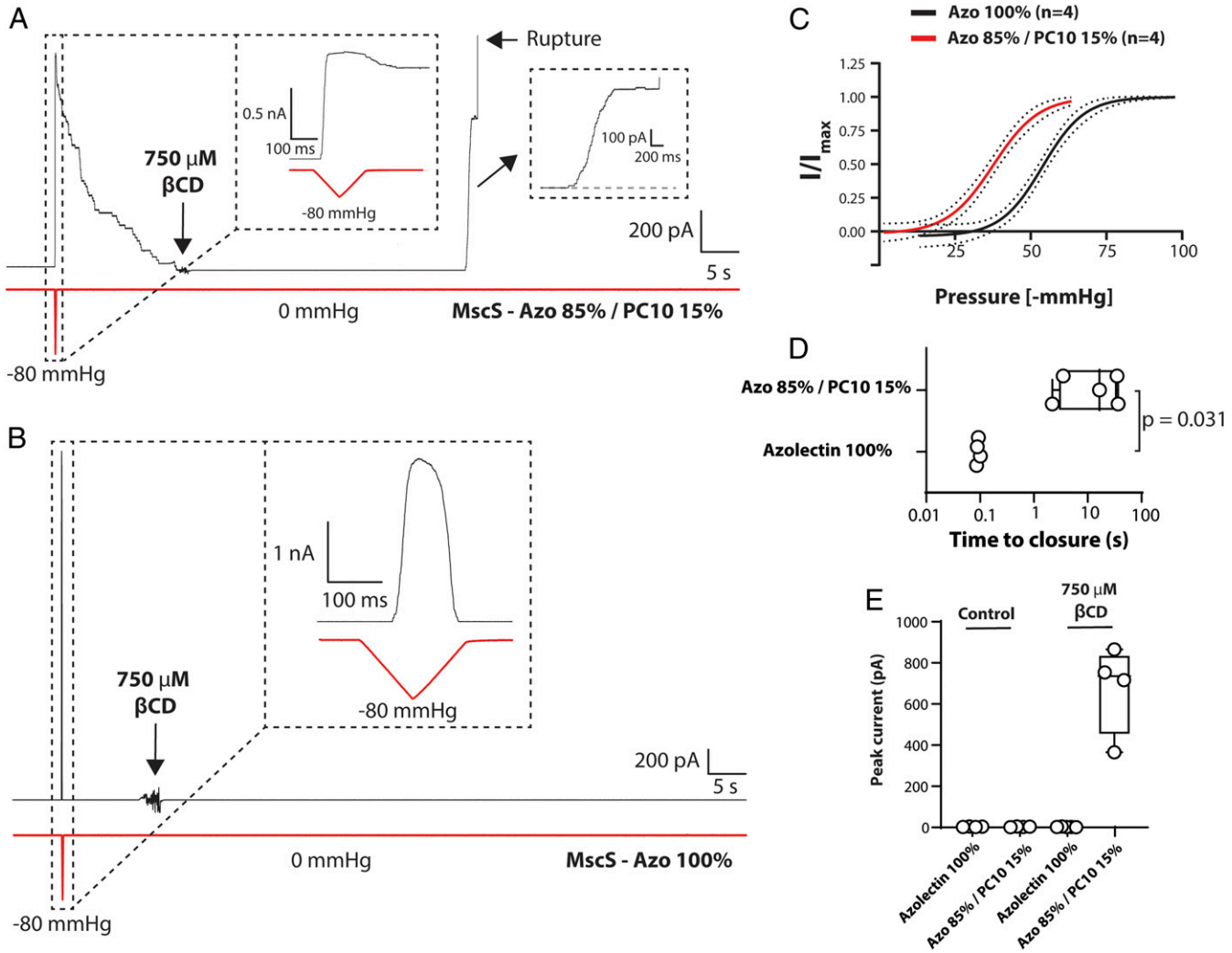

Fig. 3. The CD concentration needed to induce gating scales with the tension sensitivity of MscS. (*A*) Representative patch-clamp recording of MscS reconstituted into azolectin (Azo) liposomes containing 15% PC10 (1:200 protein:lipid ratio) at +20 mV pipette potential with the addition of 750 μM β-CD. (*B*) Representative patch-clamp recording of MscS reconstituted into pure azolectin liposomes (1:200 protein:lipid ratio) at +20 mV pipette potential with the addition of 750 μM β-CD. (*C*) Comparison of the pressure-response curves of MscS reconstituted into azolectin alone (black) and in azolectin containing 15% PC10 (red). Data are fitted with Boltzmann distribution, and dashed black lines show the 95% CI. Data were collected in response to 500-ms pressure ramps. (*D*) Quantification of the time from peak pressure applied until the last MscS closes in pure azolectin liposomes and azolectin liposomes containing 15% PC10 (*P* value determined using unpaired *t* test). (*E*) Quantification of the peak current elicited from excised liposome patches in response to perfusion with 750 μM β-CD prior to patch rupture. These results illustrate that smaller amounts of β-CD are required to activate MscS in a lipid environment in which the required tension for channel gating is lower.

shown in Fig. 1 for the Gly113Ala mutant channel in liposomes containing 30% PE18:1, the time from activation of the first channel to maximal current was substantially longer (23 ± 12 s; $n = 5$) when 5 mM β-CD was used compared to when 10 mM β-CD was used (1.17 ± 0.26 s; $n = 5$). These results suggest that MscS desensitization kinetics depend on the lipid environment.

To further illustrate this fact, we used 5-s-long subsaturating pressure pulses at 40% of the saturating pressure to normalize desensitization between patches (Fig. 4 *C–F*) (19, 67). Subsaturating pressure pulses more readily reveal MscS desensitization kinetics. In addition, desensitization is voltage-dependent and is more readily observed at negative pipette potentials than at positive pipette potentials, shown in Fig. 4 *C–E* by comparing channel activity at +60 mV and −60 mV (Fig. 4 *D–F*). While desensitization is rapid at negative pipette potentials (−60 mV) for wild-type MscS in the presence of 30% PE18:1, it is much slower in pure azolectin liposomes at the same voltage (−60 mV) as quantified by the current remaining at the end of the pressure pulse (Fig. 4 *D–G*). To prove that the changes in MscS activity in an azolectin membrane compared to that in an azolectin membrane doped with 30% PE18:1 are linked to desensitization, we again reconstituted the Gly113Ala mutant MscS that displays a vastly reduced adaptive gating behavior (23). At the same voltage (−60 mV), the Gly113Ala mutant MscS showed substantially less desensitization in an azolectin membrane that contains 30% PE18:1 (Fig. 4 *D–G*).

CDs Also Activate Reconstituted MscL. To test whether CDs can also be used to activate other structurally distinct MS channels, we chose to investigate MscL. This channel only opens under extreme membrane tension just before membranes rupture; successful CD-mediated activation of MscL would suggest that CDs would activate any membrane tension–sensitive MS channel. We coreconstituted MscS with MscL in azolectin liposomes and perfused excised patches with β-CD. Under the application of a ramp to a maximum pressure of −40 mmHg, only MscS

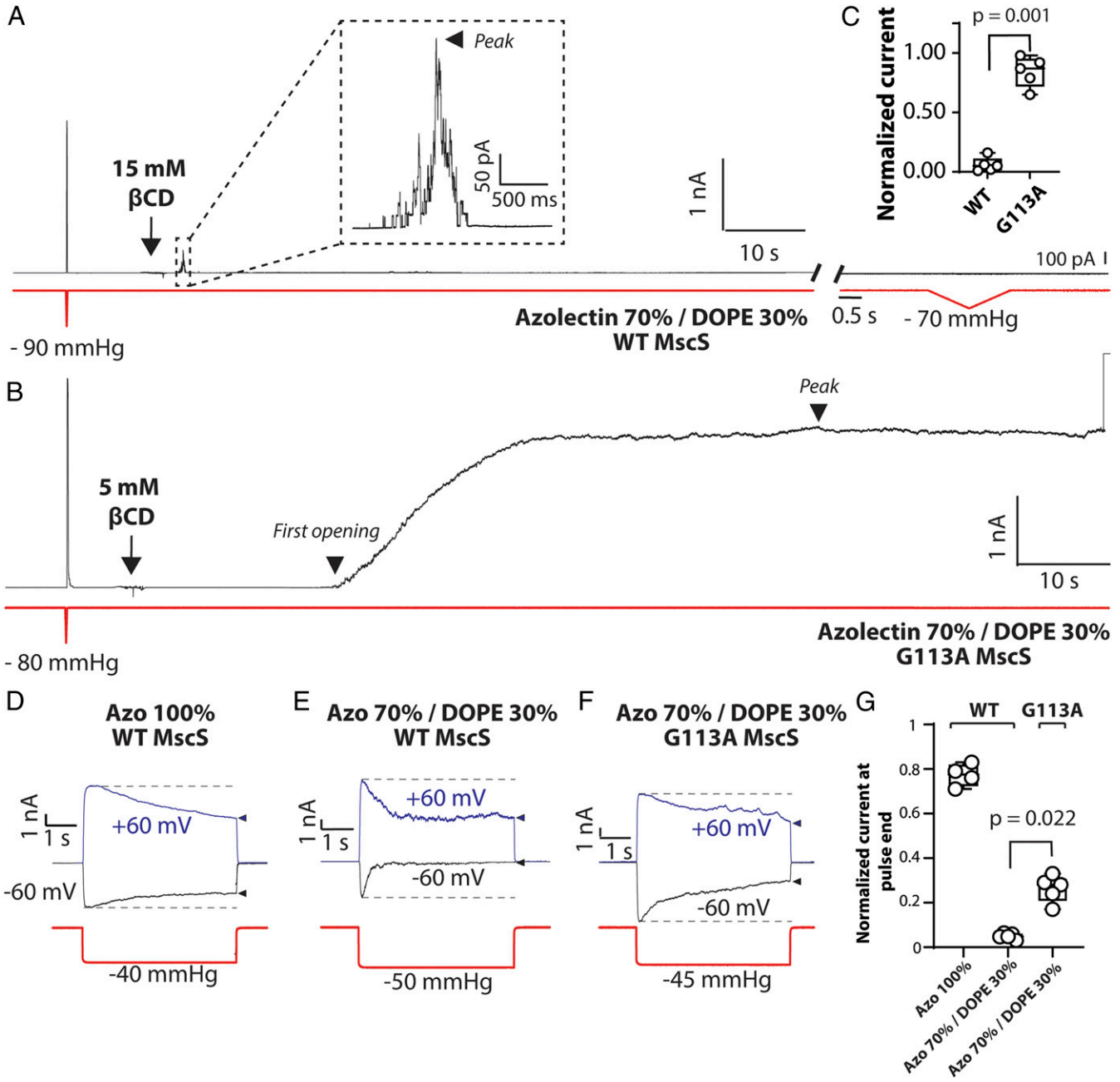

Fig. 4. CDs induce activation and subsequent desensitization of MscS, which is influenced by the lipid environment. (*A*) Representative electrophysiological recordings of wild-type (WT) MscS reconstituted into 70% azolectin (Azo) and 30% PE18:1 at +20 mV pipette potential in response to perfusion with 15 mM β-CD. After activation, the channels rapidly desensitize (*Left*) and then remain insensitive to applied negative pressure (*Right*). (*B*) Representative electrophysiological recordings of Gly113Ala mutant (G113A) MscS, a channel variant that does not desensitize, reconstituted into 70% Azo and 30% PE18:1 at +20 mV pipette potential in response to perfusion with 5 mM β-CD. Once the mutant channels are activated by lipid removal, they stay open for a long period with little to no signs of desensitization. (*C*) Minimum to maximum box and whisker plots showing normalized current from WT and Gly113Ala MscS reconstituted into 70% Azo and 30% PE18:1 treated with β-CD 5 s after the peak current was reached. Note how the WT MscS has desensitized so that no current remains, whereas Gly113Ala MscS remains open ($P < 0.0001$, *t* test). (*D*) Representative electrophysiological recordings of WT MscS reconstituted into 100% azolectin at pipette potentials of +60 mV (blue) and −60 mV (black). (*E*) Representative electrophysiological recordings of WT MscS reconstituted into 70% azolectin and 30% PE18:1 at pipette potentials of +60 mV (blue) and −60 mV (black) showing rapid desensitization at negative potentials. (*F*) Representative electrophysiological recordings of Gly113Ala mutant MscS reconstituted into 70% azolectin and 30% PE18:1 at pipette potentials of +60 mV (blue) and −60 mV (black). Note the much slower desensitization of this mutant channel compared to WT MscS, particularly at −60 mV. (*G*) Quantification of MscS desensitization as a function of lipid composition at −60 mV pipette potential by comparing the peak current to the current remaining at the end of a 5-s subsaturating pressure pulse at 40% of the saturating pressure. *P* values shown were generated using the Kruskal–Wallis test with Dunn's post hoc.

activity was recorded. To measure the membrane tension during our patch-clamp recordings resulting from the application of negative pressure and β-CD perfusion, we concomitantly imaged the rhodamine-PE18:1–containing membrane patch by confocal microscopy. Visualization of the patch demonstrated that the maximum pressure applied (−40 mmHg) generated a membrane tension of 7.1 mN/m, which was calculated using LaPlace's law by measuring the patch dome radius (64). This tension is saturating

for MscS in azolectin (10, 64, 68) but is not high enough to open MscL (64) (Fig. 5*A*). The patch was then perfused with 25 mM β-CD. Perfusion with β-CD first opened MscS and, as the MscS current saturated, the first MscL openings became evident (3× the current amplitude of MscS). Subsequently, many more MscL opened prior to patch rupture (Fig. 5*B*). Monitoring the membrane patch using confocal microscopy showed that perfusion with β-CD caused a progressive loss of the resting inward curvature (Fig. 5*B*, image *i*) until the patch became completely flat (Fig. 5*B*, image *iv*) and finally ruptured (Fig. 5*B*, image *v*), similar to the data shown in Fig. 2. The peak current from MscS and MscL are quantified in Fig. 5*C* from independent patches with and without the addition of β-CD.

β-CD–Induced Conformational Change in MscL. Given the fact that β-CD could activate MscS in azolectin liposomes and allowed cryo-EM visualization of nanodisc-embedded MscS in the desensitized state (39), we asked whether β-CD–mediated lipid removal would also affect the conformation of MscL. Wild-type MscL was purified and reconstituted into nanodiscs and subsequently treated with 100 mM β-CD for 16 h. Cryo-EM imaging and resulting 2D-class averages of the nanodisc-embedded MscL showed that β-CD treatment caused a thinning of the transmembrane region (representing the lipid bilayer surrounded by the membrane-scaffold proteins and the transmembrane domain of MscL) (Fig. 5*D* and *SI Appendix*, Fig. S3). This observation is consistent with the previously proposed gating mechanism (33) and structural dynamics (69) of MscL and suggests that β-CD–mediated removal of lipids from the nanodiscs resulted in activation of MscL. We quantified the thickness of the transmembrane region in 2D-class averages obtained with and without β-CD treatment, which revealed that nanodisc-embedded MscL treated with β-CD showed more particles with a thinner transmembrane region (Fig. 5*E*).

The Activating CD Concentration Scales with the Tension Sensitivity of MscL. To further affirm that the amount of CD necessary to activate an MS channel scales with the tension sensitivity of the channel, we made use of Gly22Ser mutant MscL that has an activation threshold close to that of MscS (70). While 5 mM β-CD activated multiple Gly22Ser MscL channels over a 90-s recording period, it failed to activate any wild-type MscL channels (Fig. 6 *A*–*C*). We also confirmed that Gly22Ser mutant MscL reconstituted into azolectin liposomes displays a leftward shift in the pressure-response curve, showing that less membrane tension is required for channel gating (Fig. 6*D*).

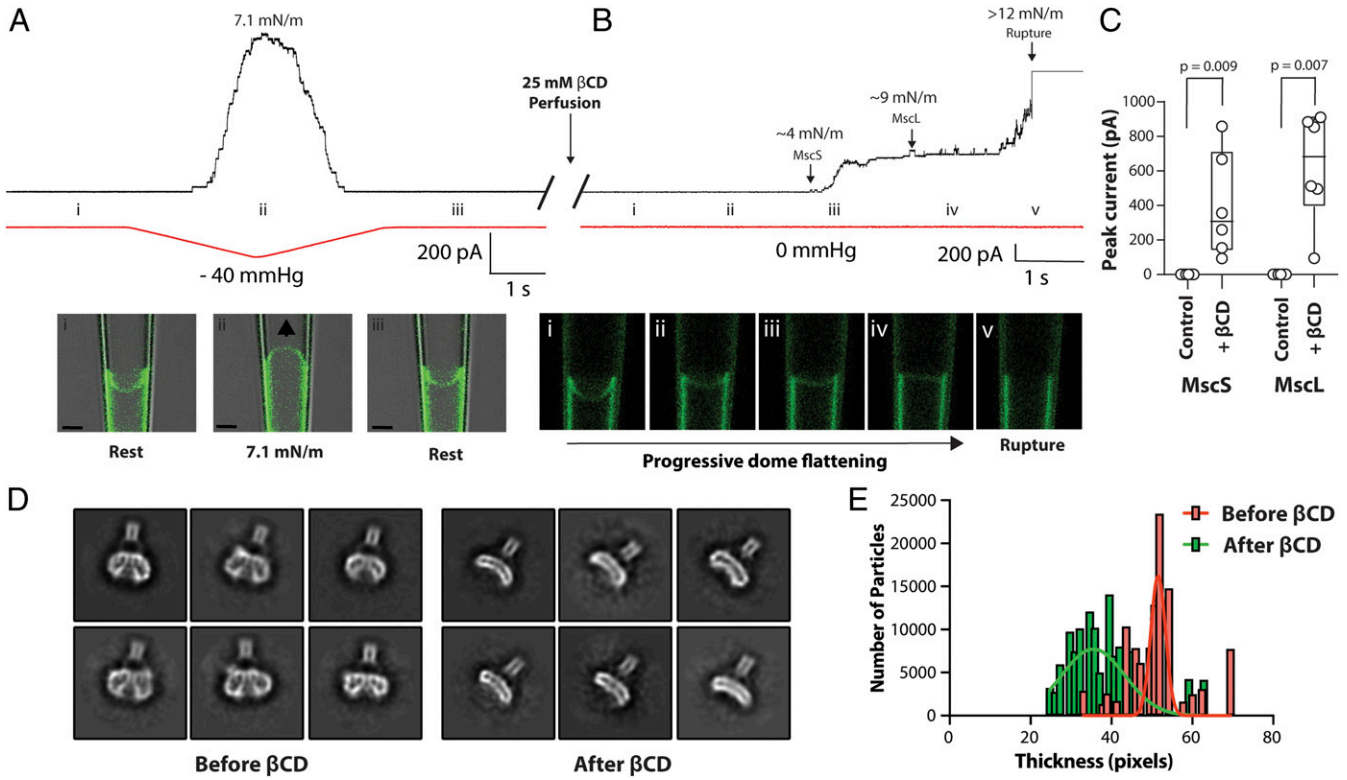

Fig. 5. CD treatment activates MscL in liposomes and causes a conformational change in nanodisc-embedded MscL. (*A*, *Top*) Exemplar trace of MscS and MscL coreconstituted into azolectin liposomes (protein:lipid ratios of 1:200 for MscS and 1:1,000 for MscL) recorded with a negative pressure ramp to a maximum of −40 mmHg in 1 s. Only MscS activity is seen, and no MscL is activated (red trace: pressure; black trace: current). (*Below*) Concomitant confocal imaging of the patch containing 0.1% of the fluorescent lipid rhodamine-PE illustrates the deformation of the membrane patch caused by the negative pressure that allowed calculation of the maximal tension generated (7.1 mN/m). (*B*, *Top*) Electrophysiological recording of the same patch after addition of 25 mM β-CD, showing first MscS activity (activation threshold: ~5 mN/m), then MscL activity (activation threshold: ~9 mN/m), and finally rupture of the membrane patch (the rupture tension of azolectin patches is >12 mN/m). (*Below*) Concomitant confocal imaging of the membrane patch shows a progressive loss of rhodamine-PE fluorescence and a flattening of the dome prior to rupture. (*C*) Minimum to maximum box and whisker plots illustrating peak current elicited by 25 mM β-CD in patches in which MscS and MscL were coreconstituted. Control represents current at rest in untreated patches. *P* value determined using unpaired *t* test. (*D*) Selected cryo-EM 2D-class averages of nanodisc-embedded MscL before and after β-CD treatment (*SI Appendix*, Fig. S3). Note the expansion and thinning of the transmembrane domain (*SI Appendix*, Fig. S3 shows how the thickness of the nanodiscs were measured). Side length of individual averages: 20 nm. (*E*) Plot of the number of nanodisc-embedded MscL particles with a given thickness of the transmembrane region before and after treatment with β-CD.

Discussion

MS channels play a key role in many mechanotransduction processes from osmoregulation in bacteria and plants (71) to touch and proprioception in mammals (72). Structurally diverse classes of MS channels (73) have been shown to respond to forces through the membrane according to the force-from-lipids mechanism (6). However, given the diversity in structure and sensitivity between members of MS channel families, it is unlikely that these channels use identical molecular mechanisms to sense membrane perturbations. Here, we show that lipid removal by CDs and their derivatives (mβ-CD) can induce membrane tension in vitro that is sufficient not only to activate MscS but also the structurally unrelated, much less tension-sensitive MscL. This result suggests that CDs will be a useful and generally applicable tool for the functional and structural interrogation of MS channel gating mechanisms.

The fact that the methylated version of β-CD can also induce sufficient membrane tension in pure phospholipid membranes is of general relevance. The increase in tension and subsequent activation of MscS by mβ-CD, which is widely used to extract cholesterol from cell membranes, suggests that experiments using high amounts of mβ-CD may have unintended effects due to the activation of MS channels (55) and demonstrates a need for appropriate controls when mβ-CD is used to remove cholesterol from native cell membranes (55).

The mechanism of CD-induced lipid removal likely involves a step of adsorption (74), and adsorption to the bilayer could make CDs activate MS channels in a similar fashion as amphipaths (6, 75). Amphipaths are thought to intercalate or adsorb into the bilayer, thus modifying the local membrane forces and inducing MS channel activation, with examples including lysolipids and small molecules like chlorpromazine (6, 75, 76). However, we have two pieces of evidence that support the conclusion that CDs increase membrane tension in vitro by lipid removal and do not act simply as amphipaths. First, cholesterol-loaded mβ-CD does not instigate MscS gating in vitro, even though lipid delivery almost certainly also involves a step in which mβ-CD adsorbs to the membrane. Second, fluorescence imaging of membrane patches containing a fluorescent lipid shows that lipid removal, as evidenced by the reduction in membrane fluorescence and the loss of the patches' resting inward curvature, happens on the same time scale as MS channel activation. This removal of lipids will result in each individual lipid having to occupy a larger surface area. Thus, providing the surface area cannot change and the lipids cannot be replenished (no lipid reservoirs), lipid removal will increase membrane tension (40, 41), which is indeed reflected in the flattening of the patch. While we have only studied reconstituted simplified membrane systems (proteoliposomes and lipid nanodiscs) that are spatially restricted and lack large lipid reservoirs, there is indeed one report that found that the incubation of cells with CDs can also cause a rise in membrane tension (51), paving the way for CDs to potentially be used in more complex, cell-based experiments (i.e., whole-cell electrophysiology). Of course, a cell can modify the surface area of its plasma membrane and use multiple ways to replenish the lipids in the plasma membrane so that the spatiotemporal influence of CDs on cellular membrane tension will require further in-depth study.

The increase in membrane tension caused by lipid removal led us to the hypothesis that in lipid environments in which MscS is more sensitive to membrane tension, fewer lipids would need to be removed by CDs to generate sufficient tension to open the channel. We tested this hypothesis using two different approaches, showing that the amount of CD necessary to activate an MS channel does indeed scale with the sensitivity of the channel to membrane tension (i.e., if a channel is more sensitive to membrane tension, less CD is required to activate it). We observed that MscS exhibited a left-shifted pressure-response curve when reconstituted into azolectin membranes doped with 15% PC10. The increased tension sensitivity of MscS in this membrane environment resulted in lower concentrations of β-CD (<1 mM) being necessary to induce gating. One caveat to this interpretation is that CDs have a preference for lipids with shorter, saturated acyl chains (56), and this could suggest that the lower amount of CDs needed in the presence of PC10 simply represents the preferential removal of PC10. However, we also demonstrated that Gly22Ser mutant MscL that is more sensitive to membrane tension (70) could also be activated by lower amounts of β-CD than wild-type MscL over similar recording periods. These results provide strong evidence that the amount of CD needed to activate an MS channel, and thus the amount of lipid that needs to be removed from the membrane, is proportional to how sensitive the channel is to membrane tension.

The β-CD–induced activation of MscS in nanodiscs and membrane patches is followed by desensitization of the channel (39). Structurally, the "desensitized state" that β-CD induces resembles what has electrophysiologically been characterized as the inactivated state (21, 22). For example, Asp62 and Arg128 form a salt bridge in the inactivated state (21, 77), and this salt bridge is seen in the cryo-EM structure of MscS in the desensitized state. Previous studies of MscS desensitization have shown that MscS is activated most robustly and fully by rapid force application in the form of a steep pressure ramp (20, 67). Slower force application reduces the number of activated channels and promotes desensitization (20, 23). Interestingly, larger amounts of β-CD are needed to activate MscS in azolectin liposomes doped with 30% PE18:1 compared with MscS in pure azolectin liposomes. This finding is consistent with the previously reported result that higher tension is required to open MscS in this lipid mixture (26), which was also shown to be the case with MscL (3). Furthermore, channel activation in this lipid mixture is followed by rapid desensitization. Using a normalized pressure protocol at subsaturating pressures, we showed that MscS desensitization is more prominent in membranes doped with 30% PE18:1 (26). A possible explanation for these observations is that lower β-CD concentrations result in a slower removal of lipids and thus a slower build-up of membrane tension. This slower increase in membrane tension is more akin to the forces generated by slower pressure ramps. Slower ramps activate some MscS, which then close and desensitize, resulting in much lower peak currents. In fact, in some scenarios, MscS has been shown to "silently" transition from the closed to a desensitized state (without entering the open state) (78), which could also explain why lower β-CD concentrations cannot activate MscS in 30% PE18:1 liposomes. This conclusion is supported by the fact that Gly113Ala mutant MscS that displays markedly reduced desensitization can be activated by lower amounts of β-CD and even in the presence of 30% PE18:1, where there is a gradual activation of all channels in the patch and no sign of any desensitization. PE lipids are the most abundant lipid type in *E. coli*, and increasing PE content within liposomes produces MscS activity that is more similar to that seen with native spheroplast membranes, which is characterized by a higher pressure threshold and more prominent desensitization (20, 79).

As in vitro studies on MS channels begin to involve more complex lipid mixtures, which mimic the lipid compositions of their native membrane environments, the differential selectivity of CD subtypes may provide some control over which lipids are removed from the membrane to induce membrane tension (56). It may be particularly important not to remove lipids that are critical for the function or mechanosensitivity of MS channels, which applies not only to structural studies on MS channels reconstituted into nanodiscs but also to functional studies, such as patch-clamp electrophysiology, planar bilayers (40), and liposome flux assays (80–82). Here, we note that it is not only MS channels that are sensitive to mechanical forces. CDs may thus

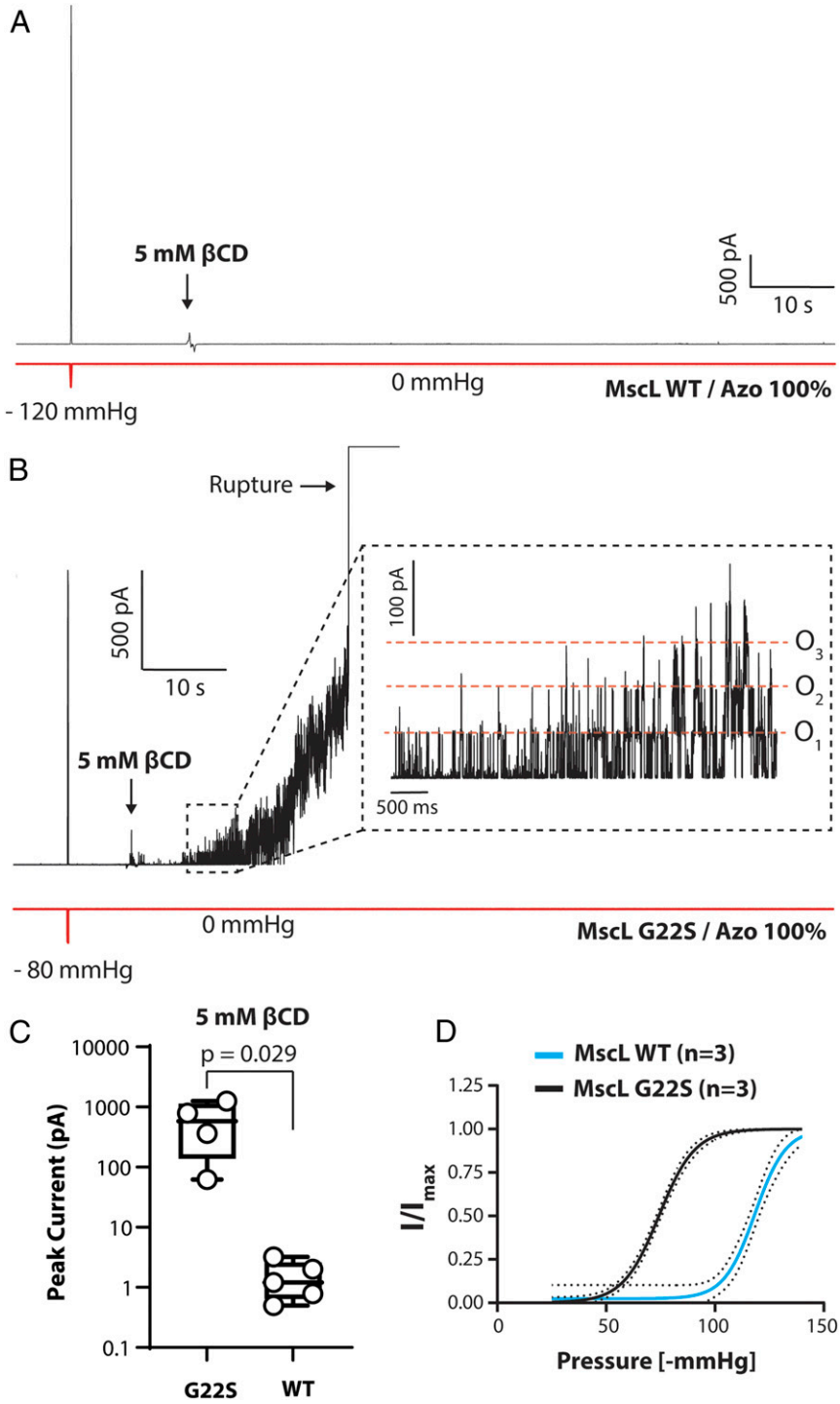

Fig. 6. CD concentration needed to activate MscL scales with the tension sensitivity of the channel. (*A*) Representative patch-clamp recording of wild-type MscL (MscL WT) reconstituted into azolectin (Azo) liposomes (1:1,000 protein:lipid ratio) at +20 mV pipette potential with the addition of 5 mM β-CD. (*B*) Representative patch-clamp recording of Gly22Ser MscL (MscL G22S), which gates at a lower membrane tension, reconstituted into azolectin liposomes (1:1,000 protein:lipid ratio) at +20 mV pipette potential with the addition of 5 mM β-CD (O_1 to O_3 = channel openings 1 through 3). (*C*) Quantification of the MscL peak current elicited from excised liposome patches in response to perfusion with 5 mM β-CD for 90 s for WT and G22S MscL (*P* value determined using unpaired *t* test). (*D*) Comparison of the pressure-response curve of WT MscL (blue) and G22S MscL (black) reconstituted into azolectin liposomes. Data are fitted with Boltzmann distribution, and dashed black lines show the 95% CI.

also prove useful for the in vitro study of other membrane proteins that are sensitive to mechanical forces (83–85). As CDs may influence membrane tension in the "whole-cell" scenario (51), CDs may also find utility in whole-cell patch clamping or Ca^{2+} imaging.

In conclusion, we present an extensive characterization of CD-induced activation of MscS in vitro in patch-clamp experiments. The three major classes of CDs, including a methylated derivative, can all rapidly activate MscS, consistent with a rise in membrane tension resulting from lipid extraction. We also show

that CDs not only activate MscS but that higher amounts perfused over the same timescale can also rapidly activate the structurally unrelated MscL. This result suggests that for both functional and structural studies, provided that sufficient CD is added and enough lipids are removed, any tension-sensitive ion channel can be activated by this approach. Given the current interest in eukaryotic MS channels and that many of these channels respond to membrane forces, CDs are likely an exceptionally useful tool for in vitro studies of this captivating class of membrane proteins.

Methods

Lipids. All lipids used in this study, soybean polar azolectin extract (catalog no. 541602), PE18:1, 1,2-dioleoyl-*sn*-glycero-3-phosphocholine (PC18:1), PC10, and 1,2-dioleoyl-*sn*-glycero-3-phosphoethanolamine-*N*-(lissamine rhodamine B sulfonyl) (rhodamine-PE18:1) were purchased from Avanti.

CDs. α-CD, β-CD, mβ-CD, and γ-CD were purchased from Sigma-Aldrich. Saturation of mβ-CD with cholesterol was carried out as described previously (86). Briefly, 100 mg cholesterol (Sigma-Aldrich) in 1:1 (v:v) chloroform:methanol was added to a glass tube, and the solvent was evaporated under an N_2 stream. A total of 10 mL 50 mM mβ-CD was added to the tube, vortexed, and then sonicated in a bath sonicator for 5 min. This 100% saturated mβ-CD:cholesterol solution was incubated on a rotating wheel at 37 °C overnight. Immediately before use, the solution was filtered through a 0.45-μm syringe filter (Millipore) to remove excess cholesterol crystals.

Purification of *E. coli* MscS and MscL. Wild-type and Gly113Ala mutant *E. coli* MscS were purified as previously reported using an N-terminal 6xHis tag (39). Briefly, MscS was expressed in *E. coli* BL21(DE3) cells, which were grown at 37 °C in lysogeny broth medium. When the culture reached an optical density $(OD)_{600}$ of ∼0.6, protein expression was induced using 1 mM isopropyl β-D-1-thiogalactopyranoside (IPTG). After 4 h at 37 °C, cells were harvested by centrifugation at 5,000 × *g* for 10 min. Cells were resuspended in 30 mM Tris-HCl, pH 7.5, 250 mM NaCl, 1% volume (vol)/vol Triton-X100, supplemented with one tablet of cOmplete Protease Inhibitor Mixture (Sigma-Aldrich) and lysed by sonication. The lysate was centrifuged at 16,000 × *g* for 30 min, incubated with 2 mL nickel resin (Qiagen), and washed with 40 mM imidazole in 30 mM Tris-HCl, pH 7.5, 250 mM NaCl, 0.02% (wt/vol) dodecyl maltoside (DDM). Protein was eluted with 250 mM imidazole in 30 mM Tris-HCl, pH 7.5, 150 mM NaCl, 0.02% DDM, concentrated using Amicon Ultra 15-mL 50-kDa centrifugal filter unit (Millipore), and loaded onto a Superdex200 column (GE Healthcare) in 30 mM Tris-HCl, pH 7.5, 150 mM NaCl, 0.02% DDM. Fractions containing MscS were pooled and used immediately for reconstitution into nanodiscs or for reconstitution and patch-clamping. For electrophysiological studies, wild-type and Gly22Ser mutant MscL with a 6xHis-tag were purified as previously reported (87). Briefly, wild-type and Gly22Ser mutant MscL were expressed in *E. coli* BL21(DE3) cells (Novagen), grown at 37 °C in lysogeny broth to an OD_{600} of ∼0.8, and then induced with 1 mM IPTG. After 3 h, the cells were centrifuged, the pellet was resuspended in phosphate-buffered saline (PBS; 10 mM Na_2HPO_4, 1.8 mM KH_2PO_4, pH 7.5, 137 mM NaCl, 2.7 mM KCl) with ∼0.02 mg/mL DNase (Sigma DN25) and 0.02% (wt/vol) phenylmethylsulfonyl fluoride (Amresco M145), and the cells were broken with a TS5/48/AE/6 A cell disrupter (Constant Systems) at 31,000 psi at 4 °C. Cell debris was removed by centrifugation (12,000 × *g* for 15 min at 4 °C), and membranes were then pelleted at 45,000 rpm in a Type 45 Ti rotor (Beckman) for 3 h at 4 °C. Membrane pellets were solubilized overnight at 4 °C with 8 mM DDM in PBS, pH 7.5. After centrifugation at 12,000 × *g* for 20 min at 4 °C, the supernatant was applied to cobalt Sepharose (Talon, 635502, Clontech). The column was washed four times with 40 mL 35 mM imidazole in PBS, pH 7.5, and protein was eluted using 500 mM imidazole in PBS, pH 7.5. The imidazole concentration was decreased using a 100-kDa Amicon-15 centrifugal filter unit (Merck Millipore) with 1 mM DDM in PBS, pH 7.5.

For structural studies, *E. coli* MscL-pET15b plasmid was purchased from Addgene (Addgene plasmid No. 92418; http://n2t.net/addgene:92418; RRID:Addgene_92418). The plasmid with an N-terminal 6xHis tag was used to transform *E. coli* BL21(DE3) cells, which were grown at 37 °C in lysogeny broth medium containing 100 μg/mL ampicillin. When the culture reached an OD_{600} of ∼0.6, protein expression was induced by adding IPTG to a final concentration of 1 mM. After another 4 h at 37 °C, cells were harvested by centrifugation at 5,000 × *g* for 10 min. Cells were resuspended and lysed by sonication in buffer containing 1% Triton-X100 in 30 mM Tris-HCl, pH 7.5, 250 mM NaCl, supplemented with one tablet of cOmplete Protease Inhibitor Mixture (Sigma-Aldrich). The lysate was clarified by centrifugation at 16,000 × *g* for 30 min at 4 °C, incubated with 2 mL nickel resin (Qiagen), and washed with 40 bead volumes of 40 mM imidazole in 30 mM Tris-HCl, pH 7.5, 250 mM NaCl, 0.02% DDM. Protein was eluted with 250 mM imidazole in 30 mM Tris-HCl, pH 7.5, 150 mM NaCl, 0.02% DDM, concentrated using Amicon Ultra 15-mL 10-kDa centrifugal filters (MilliporeSigma), and loaded onto a Superdex200 column (GE Healthcare) in 30 mM Tris-HCl, pH 7.5, 150 mM NaCl, 0.02% DDM. Fractions containing MscL were pooled and used immediately for reconstitution into nanodiscs.

The membrane-scaffold protein MSP1E3D1, which assembles nanodiscs of 13-nm diameter, with a tobacco etch virus (TEV) protease-cleavable N-terminal 6xHis tag was expressed in *E. coli* BL21(DE3) cells as described for MscL. The cells were lysed by sonication with 1% Triton-X100 in 30 mM Tris-HCl, pH 7.5, 500 mM NaCl, and supplemented with one tablet of cOmplete Protease Inhibitor Mixture (Sigma-Aldrich). After centrifugation at 16,000 × *g* for 30 min at 4 °C, the supernatant was loaded on a nickel column and the beads were washed with 20 column volumes (CV) of 40 mM imidazole in 30 mM Tris-HCl, pH 7.5, 500 mM NaCl, 1% (wt/vol) sodium cholate, followed by 20 CV of the same buffer without sodium cholate. Protein was eluted with 250 mM imidazole in 30 mM Tris-HCl, pH 7.5, 150 mM NaCl. The His tag was removed by incubation with TEV protease at a molar MSP1E3D1:TEV protease ratio of 30:1. After dialysis overnight at 4 °C against 400 mL 30 mM Tris-HCl, pH 7.5, 150 mM NaCl, the sample was loaded onto a nickel column to remove the cleaved-off His tag and the His-tagged TEV protease. The flow-through was concentrated using Amicon Ultra 15-mL 10-kDa centrifugal filters (MilliporeSigma) and loaded onto a Supderdex200 column equilibrated with 30 mM Tris-HCl, pH 7.5, 150 mM NaCl. The MSP1E3D1-containing fractions were pooled and concentrated to 4.2 mg/mL using Amicon Ultra 15-mL 10-kDa centrifugal filters (MilliporeSigma).

Reconstitution of MscL into Nanodiscs. PC18:1 was solubilized with 20 mM sodium cholate in 30 mM Tris-HCl, pH 7.5, 150 mM NaCl with sonication. MscL and MSP1E3D1 were mixed with the detergent-solubilized lipid at a molar ratio of 1:10:1000 in 12 mL 30 mM Tris-HCl, pH 7.5, 150 mM NaCl, 0.02% DDM. After 10 min, 1.5 mL of BioBeads SM-2 slurry (Bio-Rad) was added to remove the detergents. After overnight incubation with constant rotation, the BioBeads were allowed to settle by gravity. The supernatant was loaded onto a nickel column to remove the empty nanodiscs. The column was washed with 20 CV 40 mM imidazole in 30 mM Tris-HCl, pH 7.5, 150 mM NaCl, and MscL was reconstituted into nanodiscs was eluted with 250 mM imidazole in 30 mM Tris-HCl, pH 7.5, 150 mM NaCl. Samples were concentrated using Amicon Ultra 15-mL 10-kDa centrifugal filters (MilliporeSigma) and loaded onto a Superdex200 column equilibrated with 30 mM Tris-HCl, pH 7.5, 150 mM NaCl. Peak fractions containing MscL in nanodiscs were pooled and used to prepare vitrified samples for cryo-EM.

Treatment of MscL-Containing Nanodiscs with β-CD. PC18:1 nanodiscs containing MscL were incubated with 100 mM β-CD as described (39). After 16 h, the sample was loaded onto a Superdex200 column equilibrated with 30 mM Tris-HCl, pH 7.5, 150 mM NaCl. The peak fractions were pooled, concentrated using Amicon Ultra 4-mL 10-kDa centrifugal filters (MilliporeSigma) and used immediately for cryo-EM sample preparation.

EM Specimen Preparation and Data Collection. The homogeneity of samples was first examined by negative-stain EM with 0.7% (wt/vol) uranyl formate as described (88). The protein concentration was measured with a nanodrop spectrophotometer (Thermo Fisher Scientific) and adjusted to 0.2 mg/mL. Aliquots of 4 μL were applied to glow-discharged 300 mesh R1.2/1.3 Au grids (Quantifoil) using a Vitrobot Mark VI (Thermo Fisher Scientific) set at 4 °C and 100% humidity. After 5 s, grids were blotted for 5 s with a blot force of −2 and plunged into liquid nitrogen–cooled ethane.

Cryo-EM imaging was performed in the Cryo-EM Resource Center at the Rockefeller University using SerialEM (89). The data of MscL in PC18:1 nanodiscs before and after treatment with β-CD were collected on a 300-kV Titan Krios electron microscope at a nominal magnification of 28,000×, corresponding to a calibrated pixel size of 1.0 Å on the specimen level. Images were collected at a defocus range of −1.2 to −2.5 μm with a K2 Summit direct electron detector in superresolution counting mode. The "superfast mode" in SerialEM was used, in which 3 × 3 holes are exposed using beam tilt and image shift before moving the stage to the next position (90). Exposures of 10 s were dose-fractionated into 40 frames (250 ms per frame) with a dose rate of six electrons/pixel/s (∼1.38 electrons/$Å^2$/frame), resulting in a total dose of 55 electrons/$Å^2$.

Image Processing. The collected movie stacks were gain-normalized, motion-corrected, dose-weighted, and binned over 2 × 2 pixels in Motioncorr2 (91). The contrast transfer function (CTF) parameters were determined with

CTFFIND4 (92) implemented in RELION-3 (93). Particles were automatically picked with Gautomatch (94). A total of 124,656 particles were extracted from 1,828 micrographs of MscL in PC18:1 nanodiscs before β-CD treatment, and 1,763,603 particles were extracted from 4,037 micrographs for MscL in PC18:1 nanodiscs after β-CD treatment. The particles were normalized and subjected to 2D classification in RELION-3. The thickness of the transmembrane domain (TMD) was determined in all 2D classes by marking the upper and lower boundaries of the TMD and measuring the distance between the two lines (*SI Appendix*, Fig. S3).

Proteoliposome Reconstitution. Prior to reconstitution into liposomes, the 6xHis tag was cleaved from MscS with thrombin. MscS and MscL were reconstituted into liposomes with different lipid components using a modified D/R reconstitution method (95). Azolectin (soybean polar azolectin extract, Avanti) was dissolved in chloroform and mixed with lipids of interest. Fluorescent rhodamine-PE18:1 was added at 0.1% (wt/wt), and the lipid mixture was dried under N_2 flow, then suspended in D/R buffer (5 mM Hepes, pH adjusted to 7.2 using KOH, 200 mM KCl) and vortexed, followed by water-bath sonication for 15 min. Protein was added to the lipid mixture at ratios (wt/wt) of 1:200 for MscS and 1:1,000 for MscL. After a 3-h incubation with agitation at room temperature, 200 mg BioBeads (SM-2, BioRad) were added, and the sample was incubated for another 3 h at room temperature. Finally, the mixture was centrifuged at 40,000 rpm in a Beckman Type 50.2 Ti rotor for 45 min, and the lipid mixture was vacuum desiccated overnight. The proteoliposomes were rehydrated in D/R buffer overnight before use.

Electrophysiology. Proteoliposomes (0.5 μL, which equates to ∼30 to 100 ng protein–lipid mixture) were incubated in the patch-clamp buffer containing 5 mM Hepes, pH 7.2, 200 mM KCl, 40 mM $MgCl_2$ for 15 min. Symmetrical ionic solutions were used in all recordings. Single-channel currents were amplified using an Axopatch 200B amplifier (Molecular Devices). The *E. coli* MscS and MscL currents were filtered at 2 kHz and sampled at 10 kHz with a Digidata 1440A using pClamp 10 software. Negative hydrostatic pressure was applied using a high-speed pressure clamp (ALA Sciences).

Patch Fluorometry. Wild-type MscS was added to liposomes at a protein:lipid ratio (wt/wt) of 1:200 and recorded by imaging the tip of the patch pipette using a confocal microscope (LSM 700; Carl Zeiss) equipped with a water immersion objective lens (×63, NA1.15) and housed within a Faraday cage. The excised proteoliposome patches that consisted of 99.9% (wt/wt) lipids of interest and 0.1% rhodamine-PE18:1 were excited with a 555-nm laser. To improve visualization of liposome patches, the pipette tip was bent ∼28° with a microforge (MF-900; Narishige) to make it parallel to the bottom face of the recording chamber (64). The diameter of the patch dome at a given negative hydrostatic pressure was measured using the ZEN software. Tension was calculated using LaPlace's law as previously described (58, 68, 79).

Data Availability. All study data are included in the article and/or *SI Appendix*.

ACKNOWLEDGMENTS. B.M. is supported by a National Health and Medical Research Council of Australia Principal Research Fellowship (APP1135974). C.D.C. is supported by a New South Wales Health Early-Mid Career Research Fellowship. We thank M. Ebrahim, J. Sotiris, and H. Ng at the Evelyn Gruss Lipper Cryo-EM Resource Center of The Rockefeller University for assistance with data collection.

1. C. D. Cox, N. Bavi, B. Martinac, Bacterial mechanosensors. *Annu. Rev. Physiol.* **80**, 71–93 (2018).
2. C. D. Cox, N. Bavi, B. Martinac, Biophysical principles of ion-channel-mediated mechanosensory transduction. *Cell Rep.* **29**, 1–12 (2019).
3. E. Perozo, A. Kloda, D. M. Cortes, B. Martinac, Physical principles underlying the transduction of bilayer deformation forces during mechanosensitive channel gating. *Nat. Struct. Biol.* **9**, 696–703 (2002).
4. P. Blount, I. Iscla, Life with bacterial mechanosensitive channels, from discovery to physiology to pharmacological target. *Microbiol. Mol. Biol. Rev.* **84**, e00055-19 (2020).
5. C. Pliotas *et al*., The role of lipids in mechanosensation. *Nat. Struct. Mol. Biol.* **22**, 991–998 (2015).
6. B. Martinac, J. Adler, C. Kung, Mechanosensitive ion channels of *E. coli* activated by amphipaths. *Nature* **348**, 261–263 (1990).
7. I. R. Booth, P. Blount, The MscS and MscL families of mechanosensitive channels act as microbial emergency release valves. *J. Bacteriol.* **194**, 4802–4809 (2012).
8. S. I. Sukharev, P. Blount, B. Martinac, F. R. Blattner, C. Kung, A large-conductance mechanosensitive channel in *E. coli* encoded by MscL alone. *Nature* **368**, 265–268 (1994).
9. P. Moe, P. Blount, Assessment of potential stimuli for mechano-dependent gating of MscL: Effects of pressure, tension, and lipid headgroups. *Biochemistry* **44**, 12239–12244 (2005).
10. S. Sukharev, Purification of the small mechanosensitive channel of *Escherichia coli* (MscS): The subunit structure, conduction, and gating characteristics in liposomes. *Biophys. J.* **83**, 290–298 (2002).
11. I. Rowe, M. Elahi, A. Huq, S. Sukharev, The mechanoelectrical response of the cytoplasmic membrane of *Vibrio cholerae*. *J. Gen. Physiol.* **142**, 75–85 (2013).
12. B. Martinac, M. Buechner, A. H. Delcour, J. Adler, C. Kung, Pressure-sensitive ion channel in *Escherichia coli*. *Proc. Natl. Acad. Sci. U.S.A.* **84**, 2297–2301 (1987).
13. A. Kloda, B. Martinac, Molecular identification of a mechanosensitive channel in archaea. *Biophys. J.* **80**, 229–240 (2001).
14. Y. Nakayama, K. Yoshimura, H. Iida, Organellar mechanosensitive channels in fission yeast regulate the hypo-osmotic shock response. *Nat. Commun.* **3**, 1020 (2012).
15. E. S. Haswell, E. M. Meyerowitz, MscS-like proteins control plastid size and shape in *Arabidopsis thaliana*. *Curr. Biol.* **16**, 1–11 (2006).
16. E. S. Hamilton, A. M. Schlegel, E. S. Haswell, United in diversity: Mechanosensitive ion channels in plants. *Annu. Rev. Plant Biol.* **66**, 113–137 (2015).
17. C. D. Cox, Y. Nakayama, T. Nomura, B. Martinac, The evolutionary 'tinkering' of MscS-like channels: Generation of structural and functional diversity. *Pflugers Arch.* **467**, 3–13 (2015).
18. P. Koprowski, W. Grajkowski, E. Y. Isacoff, A. Kubalski, Genetic screen for potassium leaky small mechanosensitive channels (MscS) in *Escherichia coli*: Recognition of cytoplasmic β domain as a new gating element. *J. Biol. Chem.* **286**, 877–888 (2011).
19. W. Grajkowski, A. Kubalski, P. Koprowski, Surface changes of the mechanosensitive channel MscS upon its activation, inactivation, and closing. *Biophys. J.* **88**, 3050–3059 (2005).
20. B. Akitake, A. Anishkin, S. Sukharev, The "dashpot" mechanism of stretch-dependent gating in MscS. *J. Gen. Physiol.* **125**, 143–154 (2005).
21. I. Rowe, A. Anishkin, K. Kamaraju, K. Yoshimura, S. Sukharev, The cytoplasmic cage domain of the mechanosensitive channel MscS is a sensor of macromolecular crowding. *J. Gen. Physiol.* **143**, 543–557 (2014).
22. K. Kamaraju, V. Belyy, I. Rowe, A. Anishkin, S. Sukharev, The pathway and spatial scale for MscS inactivation. *J. Gen. Physiol.* **138**, 49–57 (2011).
23. B. Akitake, A. Anishkin, N. Liu, S. Sukharev, Straightening and sequential buckling of the pore-lining helices define the gating cycle of MscS. *Nat. Struct. Mol. Biol.* **14**, 1141–1149 (2007).
24. M. D. Edwards, W. Bartlett, I. R. Booth, Pore mutations of the *Escherichia coli* MscS channel affect desensitization but not ionic preference. *Biophys. J.* **94**, 3003–3013 (2008).
25. M. Boer, A. Anishkin, S. Sukharev, Adaptive MscS gating in the osmotic permeability response in *E. coli*: The question of time. *Biochemistry* **50**, 4087–4096 (2011).
26. F. Xue *et al*., Membrane stiffness is one of the key determinants of *E. coli* MscS channel mechanosensitivity. *Biochim. Biophys. Acta Biomembr.* **1862**, 183203 (2020).
27. G. Chang, R. H. Spencer, A. T. Lee, M. T. Barclay, D. C. Rees, Structure of the MscL homolog from *Mycobacterium tuberculosis*: A gated mechanosensitive ion channel. *Science* **282**, 2220–2226 (1998).
28. P. Wiggins, R. Phillips, Analytic models for mechanotransduction: Gating a mechanosensitive channel. *Proc. Natl. Acad. Sci. U.S.A.* **101**, 4071–4076 (2004).
29. R. K. Hite, X. Tao, R. MacKinnon, Structural basis for gating the high-conductance Ca^{2+}-activated K^+ channel. *Nature* **541**, 52–57 (2017).
30. R. K. Hite, R. MacKinnon, Structural titration of Slo2.2, a Na^+-dependent K^+ channel. *Cell* **168**, 390–399.e11 (2017).
31. A. Kumar *et al*., Mechanisms of activation and desensitization of full-length glycine receptor in lipid nanodiscs. *Nat. Commun.* **11**, 3752 (2020).
32. V. Vásquez, M. Sotomayor, J. Cordero-Morales, K. Schulten, E. Perozo, A structural mechanism for MscS gating in lipid bilayers. *Science* **321**, 1210–1214 (2008).
33. E. Perozo, D. M. Cortes, P. Sompornpisut, A. Kloda, B. Martinac, Open channel structure of MscL and the gating mechanism of mechanosensitive channels. *Nature* **418**, 942–948 (2002).
34. B. Corry *et al*., An improved open-channel structure of MscL determined from FRET confocal microscopy and simulation. *J. Gen. Physiol.* **136**, 483–494 (2010).
35. Y. Wang *et al*., Single molecule FRET reveals pore size and opening mechanism of a mechano-sensitive ion channel. *eLife* **3**, e01834 (2014).
36. S. G. Brohawn, E. B. Campbell, R. MacKinnon, Physical mechanism for gating and mechanosensitivity of the human TRAAK K+ channel. *Nature* **516**, 126–130 (2014).
37. W. Wang *et al*., The structure of an open form of an *E. coli* mechanosensitive channel at 3.45 A resolution. *Science* **321**, 1179–1183 (2008).
38. Z. Deng *et al*., Structural mechanism for gating of a eukaryotic mechanosensitive channel of small conductance. *Nat. Commun.* **11**, 3690 (2020).
39. Y. Zhang *et al*., Visualizing the mechanosensitive ion channel MscS under membrane tension. *Nature* (2021).
40. M. V. Clausen, V. Jarerattanachat, E. P. Carpenter, M. S. P. Sansom, S. J. Tucker, Asymmetric mechanosensitivity in a eukaryotic ion channel. *Proc. Natl. Acad. Sci. U.S.A.* **114**, E8343–E8351 (2017).
41. M. Staykova, D. P. Holmes, C. Read, H. A. Stone, Mechanics of surface area regulation in cells examined with confined lipid membranes. *Proc. Natl. Acad. Sci. U.S.A.* **108**, 9084–9088 (2011).
42. G. Crini, Review: A history of cyclodextrins. *Chem. Rev.* **114**, 10940–10975 (2014).
43. K. A. Connors, The stability of cyclodextrin complexes in solution. *Chem. Rev.* **97**, 1325–1358 (1997).

44. S. S. Braga, Cyclodextrins: Emerging medicines of the new millennium. *Biomolecules* **9**, 801 (2019).
45. S. B. Carneiro *et al*., Cyclodextrin¯drug inclusion complexes: In vivo and in vitro approaches. *Int. J. Mol. Sci.* **20**, 642 (2019).
46. L. Szente, É. Fenyvesi, Cyclodextrin-lipid complexes: Cavity size matters. *Struct. Chem.* **28**, 479–492 (2017).
47. A. Vahedi, P. Bigdelou, A. M. Farnoud, Quantitative analysis of red blood cell membrane phospholipids and modulation of cell-macrophage interactions using cyclodextrins. *Sci. Rep.* **10**, 15111 (2020).
48. J. B. Startek *et al*., Mouse TRPA1 function and membrane localization are modulated by direct interactions with cholesterol. *eLife* **8**, e46084 (2019).
49. S. A. Sanchez, G. Gunther, M. A. Tricerri, E. Gratton, Methyl-β-cyclodextrins preferentially remove cholesterol from the liquid disordered phase in giant unilamellar vesicles. *J. Membr. Biol.* **241**, 1–10 (2011).
50. M. Denz *et al*., Interaction of fluorescent phospholipids with cyclodextrins. *Chem. Phys. Lipids* **194**, 37–48 (2016).
51. A. Biswas, P. Kashyap, S. Datta, T. Sengupta, B. Sinha, Cholesterol depletion by MβCD enhances cell membrane tension and its variations-reducing integrity. *Biophys. J.* **116**, 1456–1468 (2019).
52. J. C. Debouzy *et al*., Mechanism of alpha-cyclodextrin induced hemolysis. 2. A study of the factors controlling the association with serine-, ethanolamine-, and choline-phospholipids. *J. Pharm. Sci.* **87**, 59–66 (1998).
53. S. Mahammad, I. Parmryd, Cholesterol depletion using methyl-β-cyclodextrin. *Methods Mol. Biol.* **1232**, 91–102 (2015).
54. P. Ridone *et al*., Disruption of membrane cholesterol organization impairs the activity of PIEZO1 channel clusters. *J. Gen. Physiol.* **152**, e201912515 (2020).
55. R. Zidovetzki, I. Levitan, Use of cyclodextrins to manipulate plasma membrane cholesterol content: Evidence, misconceptions and control strategies. *Biochim. Biophys. Acta* **1768**, 1311–1324 (2007).
56. Z. Huang, E. London, Effect of cyclodextrin and membrane lipid structure upon cyclodextrin-lipid interaction. *Langmuir* **29**, 14631–14638 (2013).
57. A. Ikeda, R. Funada, K. Sugikawa, Different stabilities of liposomes containing saturated and unsaturated lipids toward the addition of cyclodextrins. *Org. Biomol. Chem.* **14**, 5065–5072 (2016).
58. C. D. Cox *et al*., Removal of the mechanoprotective influence of the cytoskeleton reveals PIEZO1 is gated by bilayer tension. *Nat. Commun.* **7**, 10366 (2016).
59. R. Syeda *et al*., Piezo1 channels are inherently mechanosensitive. *Cell Rep.* **17**, 1739–1746 (2016).
60. S. G. Brohawn, Z. Su, R. MacKinnon, Mechanosensitivity is mediated directly by the lipid membrane in TRAAK and TREK1 K+ channels. *Proc. Natl. Acad. Sci. U.S.A.* **111**, 3614–3619 (2014).
61. S. E. Murthy *et al*., OSCA/TMEM63 are an evolutionarily conserved family of mechanically activated ion channels. *eLife* **7**, e41844 (2018).
62. M. Zhang *et al*., Structure of the mechanosensitive OSCA channels. *Nat. Struct. Mol. Biol.* **25**, 850–858 (2018).
63. B. Reddy, N. Bavi, A. Lu, Y. Park, E. Perozo, Molecular basis of force-from-lipids gating in the mechanosensitive channel MscS. *eLife* **8**, e50486 (2019).
64. T. Nomura *et al*., Differential effects of lipids and lyso-lipids on the mechanosensitivity of the mechanosensitive channels MscL and MscS. *Proc. Natl. Acad. Sci. U.S.A.* **109**, 8770–8775 (2012).
65. C. D. Cox *et al*., Selectivity mechanism of the mechanosensitive channel MscS revealed by probing channel subconducting states. *Nat. Commun.* **4**, 2137 (2013).
66. M. Bogdanov *et al*., Phospholipid distribution in the cytoplasmic membrane of Gram-negative bacteria is highly asymmetric, dynamic, and cell shape-dependent. *Sci. Adv.* **6**, eaaz6333 (2020).
67. U. Çetiner, A. Anishkin, S. Sukharev, Spatiotemporal relationships defining the adaptive gating of the bacterial mechanosensitive channel MscS. *Eur. Biophys. J.* **47**, 663–677 (2018).
68. T. Nomura, C. D. Cox, N. Bavi, M. Sokabe, B. Martinac, Unidirectional incorporation of a bacterial mechanosensitive channel into liposomal membranes. *FASEB J.* **29**, 4334–4345 (2015).
69. N. Bavi *et al*., Structural dynamics of the MscL C-terminal domain. *Sci. Rep.* **7**, 17229 (2017).
70. K. Yoshimura, A. Batiza, M. Schroeder, P. Blount, C. Kung, Hydrophilicity of a single residue within MscL correlates with increased channel mechanosensitivity. *Biophys. J.* **77**, 1960–1972 (1999).
71. J. H. Naismith, I. R. Booth, Bacterial mechanosensitive channels—MscS: Evolution's solution to creating sensitivity in function. *Annu. Rev. Biophys.* **41**, 157–177 (2012).
72. B. Martinac, C. D. Cox, "Mechanosensory transduction: Focus on ion channels" in *Comprehensive Biophysics,* E. Egelman, Ed. (Elsevier, 2017), vol. 7, pp. 108–141.
73. P. Jin, L. Y. Jan, Y. N. Jan, Mechanosensitive ion channels: Structural features relevant to mechanotransduction mechanisms. *Annu. Rev. Neurosci.* **43**, 207–229 (2020).
74. C. A. López, A. H. de Vries, S. J. Marrink, Molecular mechanism of cyclodextrin mediated cholesterol extraction. *PLOS Comput. Biol.* **7**, e1002020 (2011).
75. C. D. Cox, P. A. Gottlieb, Amphipathic molecules modulate PIEZO1 activity. *Biochem. Soc. Trans.* **47**, 1833–1842 (2019).
76. J. A. Lundbaek, R. E. Koeppe II, O. S. Andersen, Amphiphile regulation of ion channel function by changes in the bilayer spring constant. *Proc. Natl. Acad. Sci. U.S.A.* **107**, 15427–15430 (2010).
77. T. Nomura, M. Sokabe, K. Yoshimura, Interaction between the cytoplasmic and transmembrane domains of the mechanosensitive channel MscS. *Biophys. J.* **94**, 1638–1645 (2008).
78. V. Belyy, A. Anishkin, K. Kamaraju, N. Liu, S. Sukharev, The tension-transmitting 'clutch' in the mechanosensitive channel MscS. *Nat. Struct. Mol. Biol.* **17**, 451–458 (2010).
79. S. Shaikh, C. D. Cox, T. Nomura, B. Martinac, Energetics of gating MscS by membrane tension in azolectin liposomes and giant spheroplasts. *Channels (Austin)* **8**, 321–326 (2014).
80. C. Cabanos, M. Wang, X. Han, S. B. Hansen, A soluble fluorescent binding assay reveals PIP_2 antagonism of TREK-1 channels. *Cell Rep.* **20**, 1287–1294 (2017).
81. Z. Su, E. C. Brown, W. Wang, R. MacKinnon, Novel cell-free high-throughput screening method for pharmacological tools targeting K+ channels. *Proc. Natl. Acad. Sci. U.S.A.* **113**, 5748–5753 (2016).
82. N. Mukherjee *et al*., The activation mode of the mechanosensitive ion channel, MscL, by lysophosphatidylcholine differs from tension-induced gating. *FASEB J.* **28**, 4292–4302 (2014).
83. J. Kim *et al*., Topological adaptation of transmembrane domains to the force-modulated lipid bilayer is a basis of sensing mechanical force. *Curr. Biol.* **30**, 1614–1625.e1615 (2020).
84. J. Xu *et al*., GPR68 senses flow and is essential for vascular physiology. *Cell* **173**, 762–775.e16 (2018).
85. S. Erdogmus *et al*., Helix 8 is the essential structural motif of mechanosensitive GPCRs. *Nat. Commun.* **10**, 5784 (2019).
86. A. E. Christian, M. P. Haynes, M. C. Phillips, G. H. Rothblat, Use of cyclodextrins for manipulating cellular cholesterol content. *J. Lipid Res.* **38**, 2264–2272 (1997).
87. K. R. Rosholm *et al*., Activation of the mechanosensitive ion channel MscL by mechanical stimulation of supported Droplet-Hydrogel bilayers. *Sci. Rep.* **7**, 45180 (2017).
88. M. Ohi, Y. Li, Y. Cheng, T. Walz, Negative staining and image classification—Powerful tools in modern electron microscopy. *Biol. Proced. Online* **6**, 23–34 (2004).
89. D. N. Mastronarde, Automated electron microscope tomography using robust prediction of specimen movements. *J. Struct. Biol.* **152**, 36–51 (2005).
90. A. Cheng *et al*., High resolution single particle cryo-electron microscopy using beam-image shift. *J. Struct. Biol.* **204**, 270–275 (2018).
91. S. Q. Zheng *et al*., MotionCor2: Anisotropic correction of beam-induced motion for improved cryo-electron microscopy. *Nat. Methods* **14**, 331–332 (2017).
92. A. Rohou, N. Grigorieff, CTFFIND4: Fast and accurate defocus estimation from electron micrographs. *J. Struct. Biol.* **192**, 216–221 (2015).
93. J. Zivanov *et al*., New tools for automated high-resolution cryo-EM structure determination in RELION-3. *eLife* **7**, e42166 (2018).
94. Gautomatch, Version 0.56. https://www2.mrc-lmb.cam.ac.uk/research/locally-developed-software/zhang-software/#gauto. Accessed 10 August 2021.
95. C. C. Häse, A. C. Le Dain, B. Martinac, Purification and functional reconstitution of the recombinant large mechanosensitive ion channel (MscL) of *Escherichia coli*. *J. Biol. Chem.* **270**, 18329–18334 (1995).